A&A 672, A7 (2023)
https://doi.org/10.1051/0004-6361/202244887

Astronomy & Astrophysics

A horn-coupled millimetre-wave on-chip spectrometer based on lumped-element kinetic inductance detectors

U. Chowdhury[1,2], F. Levy-Bertrand[1,2], M. Calvo[1,2], J. Goupy[1,2,3], and A. Monfardini[1,2]

[1] Univ. Grenoble Alpes, CNRS, Grenoble INP, Institut Néel, 25 rue des Martyrs, 38042 Grenoble, France
e-mail: monfardini@neel.cnrs.fr
[2] Groupement d'Intérêt Scientifique KID, 38042 Grenoble and 38400 Saint-Martin-d'Hères, France
[3] Institut de RadioAstronomie Millimétrique (IRAM), 300 rue de la piscine, 38400 Saint-Martin-d'Hères, France

Received 5 September 2022 / Accepted 5 February 2023

ABSTRACT

Context. Millimetre-wave astronomy is an important tool for both general astrophysics studies and cosmology. A large number of unidentified sources are being detected by the large field-of-view continuum instruments operating on large telescopes.
Aims. New smart focal planes are needed to bridge the gap between the large bandwidth continuum instruments operating on single-dish telescopes and high spectral and angular resolution interferometers (e.g. ALMA in Chile and NOEMA in France). The aim is to perform low to medium spectral resolution observations and select a lower number of potentially interesting sources (i.e. high-redshift galaxies) for further follow-up.
Methods. We have designed, fabricated, and tested an innovative on-chip spectrometer sensitive in the 85–110 GHz range. It contains 16 channels, each of which covers a frequency band of about 0.2 GHz. A conical horn antenna coupled to a slot in the ground plane collects the radiation and guides it to a millimetre-wave microstrip transmission line placed on the other side of the mono-crystalline substrate. The millimetre-wave line is coupled to a filter-bank spectrometer. Each filter is capacitively coupled to a lumped-element kinetic inductance detector (LEKID). The microstrip configuration provides the benefit of low loss, due to the mono-crystalline substrate, and protects the LEKIDs from illumination by stray un-filtered light.
Results. The prototype spectrometer exhibits a spectral resolution $R = \lambda/\Delta\lambda \approx 300$. The optical noise equivalent power is in the low 10^{-16} W Hz$^{-1/2}$ range for an incoming power of about 0.2 pW per channel. The device is polarisation-sensitive, with a cross-polarisation lower than 1% for the best channels.

Key words. instrumentation: detectors – instrumentation: spectrographs

1. Introduction

In the framework of millimetre-wave astronomy, on-chip spectrometers, with their compact design, aim to achieve intermediate spectral resolution (i.e. $R = \lambda/\Delta\lambda = 100$–$1000$), preserving the high sensitivity typical of direct detectors. A key advantage compared to existing Fourier transform spectrometers (FTSs; CONCERTO Collaboration 2020; Monfardini & Lagache 2021) is the reduction of the optical background power per channel, with a gain in the achievable photon-limited noise that can theoretically approach $1/\sqrt{R}$. In addition, the optical design is enormously simplified. The main drawback is the need for at least one readout channel per spectral band. For this reason, focal planes equipped with a large number (i.e. thousands) of on-chip spectrometers are impossible due to the limits set by current detector readout technology.

On-chip spectrometers with integrated kinetic inductance detectors (KIDs) have already been proposed and are under development, including Micro-Spec (Volpert et al. 2022), SPT-SLIM (Karkare et al. 2022), and WSPEC (Bryan et al. 2015), and on-chip FTSs (Faramarzi et al. 2020) are being fabricated and tested, including SuperSpec (Karkare et al. 2020) and DESHIMA (Endo et al. 2019). The Micro-Spec spectrometer was designed for a resolution of around 512 in the 420–540 GHz band. The SuperSpec device demonstrated a resolution of ∼275 in the 255–278 GHz band. The DESHIMA spectrometer on the ASTE 10-m telescope achieved a bandwidth of 45 GHz centred around 350 GHz with a resolution of 380.

In this work, we present the design, fabrication, and first tests of an on-chip spectrometer with lumped-element kinetic inductance detectors (LEKIDs). Our on-chip millimetre-wave kinetic inductance detector (OMKID) spectrometer targets the 85–110 GHz atmospheric window. The concept is similar to that of the spectrometers mentioned above. The main differences are: (a) the frequency band; (b) optical coupling via a horn antenna, allowing better control of the beam; and (c) a microstrip configuration with a mono-crystalline sapphire dielectric that simplifies the processing, ensures low radio frequency losses, and protects the device from spurious (i.e. unfiltered) radiation. The OMKID fabrication process has been designed to be compatible with large composite (imaging and spectroscopy) focal planes. That will allow the large mapping speed to be preserved and, at the same time, the smaller and/or selected portions of the overall field of view to be spectroscopically imaged.

2. Design and fabrication

Our OMKID spectrometer has been designed and fabricated on a 2-inch mono-crystalline C-plane sapphire substrate. A schematic view is presented in Fig. 1. The incoming signal, centred around 90 GHz, is collected by a smooth conical horn antenna with a flare angle of 30°. The 12 mm long horn ends in a portion of a cylindrical waveguide with a diameter of 2.5 mm. The cut-off frequency is around 70 GHz, and the antenna is expected to be single-mode (TE_{11}) until the onset of the TM_{01} mode above

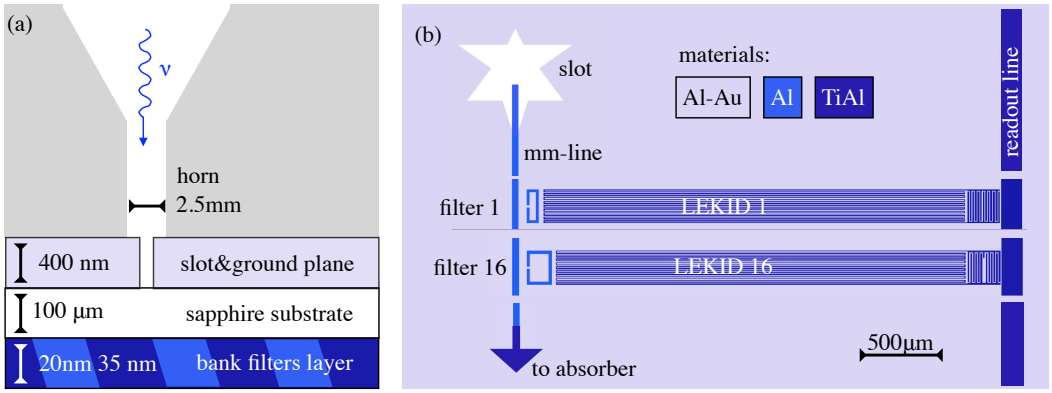

Fig. 1. OMKID spectrometer schematic. The spectrometer targets the 85–110 GHz range with 16 channels. (*a*) *Side view*. The radiation is collected through a horn waveguide, a slot termination, a sapphire substrate, and a millimetre-wave transmission line. (*b*) *Top view*. The c-shaped filters pick up the signal from the millimetre-wave line. The filtered signal is absorbed by the LEKIDs, which are made of TiAl (with a superconducting gap of 70 GHz). The resonance frequencies of the LEKIDs are monitored with the gigahertz readout line.

91 GHz. The waveguide itself is terminated by a star-shaped slot etched in the ground plane that is deposited on the back side of the sapphire substrate. The slot is fed by a millimetre-wave microstrip line placed on the front side. The transmission line guides the signal up to the filters and terminates in an absorber. The absorber is intended to suppress possible standing waves. The superconducting filters, placed on the same plane, are each coupled to a LEKID that dissipates the millimetre-wave signal via the generation of quasi-particles. The resonance frequencies of the LEKID are affected by the change in their kinetic inductance. The 16 channels are all read out via frequency-multiplexing by a single microstrip readout line, which couples to an IN/OUT pair of coaxial cables. The readout rate for the OMKID tests is fixed at 46 Hz.

Our star-shaped slot is only one among the possible waveguide-microstrip transitions. Similar fractal designs that operate at lower frequencies and as free-space coupled antennas have been proposed (Liu et al. 2020). From our simulations, after matching the microstrip feed, we estimate an operational range between 85 and 110 GHz with a simulated efficiency of 15–45% across the band. The waveguide-microstrip transition is thus the bottleneck of our design in terms of overall bandwidth.

The superconducting filters are properly shaped half-wave planar resonators. The length of each of the 16 filters is varied to cover the 85–110 GHz range. The coupling quality factor of each filter with the millimetre-wave microstrip can be adjusted to target a bandwidth of about 0.2 GHz. The notable c-shape of the filters is intended to maximise the current next to the LEKID and optimise the dissipation efficiency in the detector.

Each LEKID consists of a meandered inductor and an interdigitated capacitor. The resonant frequency is tuned by adjusting the length of the meander (L) and one of the fingers of the capacitor (C). The resonance frequencies range between 1.5 GHz and 1.8 GHz. The internal quality factor, Q_i (material), and the coupling quality factor, Q_c (design), are both in the 10^5 range. The LEKIDs, as in our standard imaging devices (Adam et al. 2018), are coupled to a 50 Ω microstrip readout line.

Three types of superconducting materials were used to fabricate the OMKID: there is a pure aluminum layer (20 nm thick), a titanium-aluminum bilayer (10 nm/25 nm thick), and an aluminum layer with a gold overlayer (200 nm/200 nm thick). The pure aluminum superconductor (Al) is a lossless conductor for frequencies below its superconducting gap frequency, $2\Delta_{Al}/h \sim 110$ GHz. It is used for the (lossless) millimetre-wave microstrip and the filters and is patterned via standard UV lithography and lift-off. The titanium-aluminum bilayer (TiAl) is used to absorb radiation at frequencies higher than its superconducting gap frequency, $2\Delta_{TiAl}/h \sim 70$ GHz (Catalano et al. 2015). It is used for the LEKID and the absorber. To ensure the repeatability of the LEKID coupling quality factor, Q_c, against possible lithography misalignments, the TiAl bilayer is also used for the gigahertz microstrip readout line. This layer is also patterned using standard UV lithography followed by diluted HF etching. The aluminum covered with Au is used for the ground plane on the back side of the substrate. The Au layer is crucial to ensuring a good thermalisation of the device (and thus a fast time constant).

3. Experimental set-up

The on-chip spectrometer is mounted in a custom optical dilution refrigerator (millimetre-wave camera) with a base temperature of about 80 mK. The camera is directly derived from the Néel IRAM KID Arrays (NIKA) instrument (Monfardini et al. 2011). The cold optics is composed of three high-density polyethylene smooth lenses (L1, L2, and L3). L1 is located at room temperature and coincides with the cryostat vacuum isolation window. L2 is mounted on the screen at a temperature of about 4 K, and the final lens, L3, is installed at the coldest stage just in front of the OMKID horn. Several custom low-pass filters installed on the radiation screens at 100 K, 50 K, 4 K, 1 K, and 0.1 K ensure an optimal rejection of the out-of-band radiation. The background on the device is set by the diameter of the cold (0.1 K) pupil lying between L2 and L3.

For characterisation, two radiation sources have been used: (i) a room-temperature black body (bb-300K) or a mirror allowing one to 'look inside' the cryostat, for an equivalent background temperature approaching 0 K (bb-0K); and (ii) a commercial millimetre-wave source coupled to a pyramidal emission horn (mm). The millimetre-wave source is polarised and can be set in the range 75–110 GHz with hertz-like frequency precision. It is, however, not calibrated in intensity, requiring a relative comparison with a well-known and modelled black body.

The signal per channel of the spectrometer is defined as the frequency shift of the corresponding LEKID. In a previous publication, we demonstrated the linear proportionality between the absorbed power and the frequency shift (Swenson et al. 2010). The frequency shift of the LEKID is measured either with a

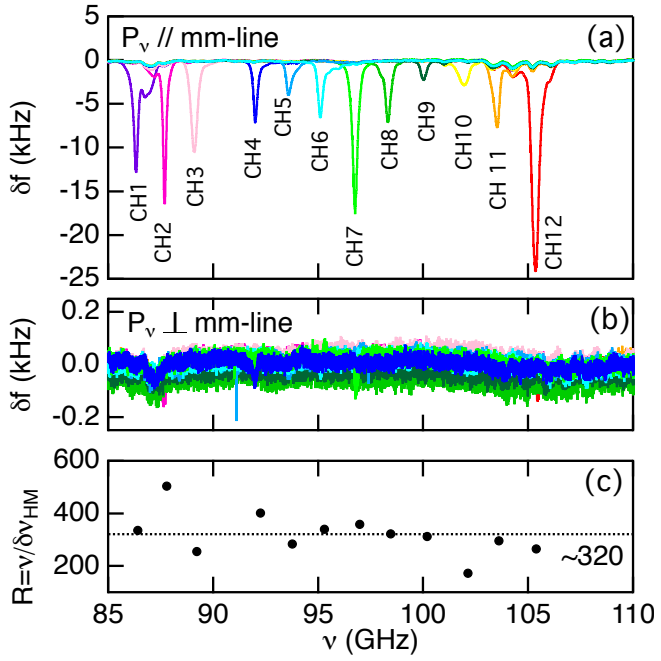

Fig. 2. OMKID spectrometer channel responses. Frequency shift of the LEKID per channel as a function of the radiation frequency: (*a*) for a polarisation of the millimetre source parallel to the millimetre-wave line and (*b*) for the perpendicular polarisation. (*c*) Spectral resolution per channel.

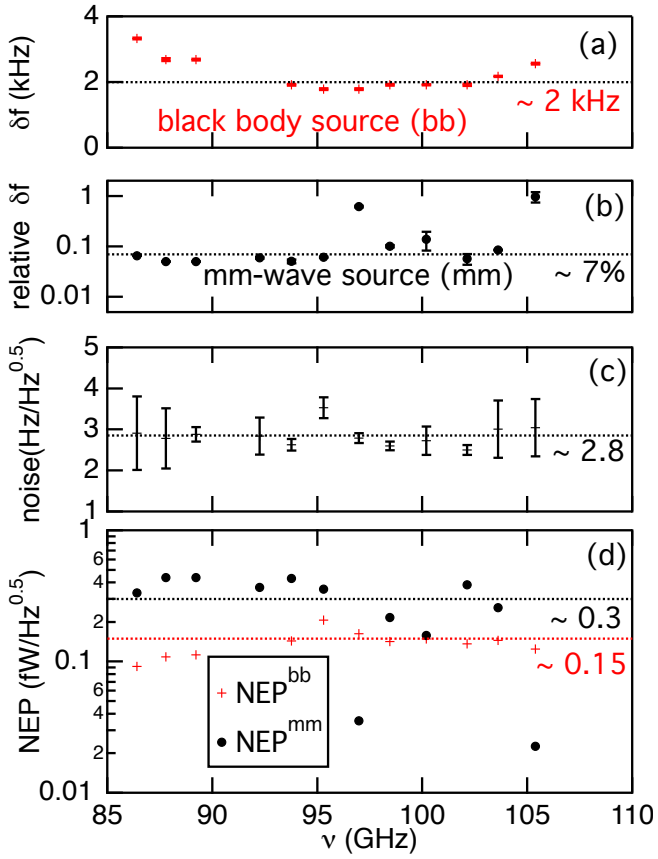

Fig. 3. NEP estimation. As a function of the channel frequency: (*a*) LEKID frequency shift for illuminations with black-body sources at 300 K and 0 K; and (*b*) LEKID relative frequency shift for an illumination with the millimetre-wave source. Normalisation is with respect to state-of-the art NIKA pixels (see text for more details). (*c*) LEKID noise spectral density at 10 Hz. (*d*) NEP estimated with the black-body source illumination (bb) or with the millimetre-wave source (mm).

vector network analyzer or using dedicated multiplexing electronics (Bourrion et al. 2013), synchronised with the millimetre source.

4. Results and discussion

Figure 2 displays the OMKID spectrometer channel responses. Twelve out of the sixteen designed channels are functional. For future devices, we have optimised a standard procedure that provides a fabrication yield of above 90%. As expected from simulations, the device is polarisation selective. Down to the noise level, no signal is detected for a polarisation perpendicular to the millimetre-wave line. The upper limit on the cross-polarisation is only 0.8% for the best channel (#12).

Figure 3 shows the measured optical noise equivalent power (NEP) per channel and the elements used to evaluate it. The NEP corresponds to the power producing a signal-to-noise ratio of one in a 1 Hz output bandwidth. It is calculated as

$$\mathrm{NEP} = \frac{\Delta W_{\mathrm{opt}} N}{\delta f}, \tag{1}$$

where δf is the frequency shift of the LEKID generated by the change in the optical load, ΔW_{opt} (the power to be detected), and N is the noise spectral density. As explained previously, the millimetre-wave source intensity is not calibrated. Thus, a direct evaluation of the optical load for an illumination with the millimetre source is impossible. To circumvent this difficulty, we used two different approaches to evaluate the NEP: (i) a standard method with an illumination with a black-body source (bb; Catalano et al. 2015, 2020; Levy-Bertrand et al. 2021) and (ii) a new method with an illumination with the millimetre-wave source (mm) and a comparison with an already characterised matrix of LEKIDs.

In the first approach we measured the frequency shift per channel for the 0–300 K temperature change of the black-body source (Fig. 3, panel a). We estimated the corresponding change in the optical load using three-dimensional ray-tracing software, where the inputs are the spectral luminescence of the black-body source, the geometry of the cryostat (the apertures, the distances, and the curvatures and materials of the lenses) and an effective collecting surface of the horn of about 30 mm^2. Usually, the optical load is evaluated by incorporating the real spectral responses. Here, the spectral responses measured with the millimetre-wave source show a channel response of about –10 kHz over a 0.4 GHz band (on average) and a hardly visible background of about –150 Hz (see Fig. 2, panel a). The background response is most probably due to stray light directly absorbed by the LEKIDs. The black-body source illuminates the LEKIDs over the 70–120 GHz band, from the TiAl superconducting gap frequency up to the low pass filter frequency. Thus, the measured frequency shift is a result of the channel response and the background response. Making the simplified assumption of a constant illumination power over the whole band for both sources, we estimate that the background contributes to about half the total response. In order to compensate for the over-evaluation of the channel frequency shift, we estimated the optical load for a 1 GHz band. The optical load varies from 75 fW at 80 GHz to 105 fW at 100 GHz for a single polarisation. In order to be conservative,

we used $\Delta W_{\rm opt} \sim 105$ fW. This value, together with the measure of the noise spectral density at 10 Hz (Fig. 3, panel c), leads to $\mathrm{NEP}^{\rm bb} \sim 0.15$ fW Hz$^{-0.5}$ (panel *d*).

In the second approach, we employed the millimetre-wave source to illuminate the OMKID and compared its response with that of a well-characterised NIKA-like imaging array made of the same TiAl material (Catalano et al. 2015, 2020). The NIKA array was characterised using a standard method with a black-body source and an optical load of about 0.4 pW. The optical NEP of the NIKA array is, on average, 2.2×10^{-17} W Hz$^{-0.5}$. The noise of the NIKA device is in the 1–3 Hz Hz$^{-0.5}$ range. We measured, using the same instrument and optical configuration, the spectral response with the millimetre source for both the NIKA array and the OMKID spectrometer. For each channel, we evaluated the relative frequency shift as the ratio of the signal of the OMKID to that of the NIKA array, both measured at the peak frequency of the channel considered (Fig. 3, panel b). A geometrical correction factor has been applied, equal to the ratio of the effective collecting surface of the horn ($\approx$30 mm^2) to the surface of the NIKA pixels (5.3 mm^2). The quantum efficiency (QE) is defined as the ratio between the number of detected photons and the number of photons hitting the detector itself. Assuming an ideal 100% QE for the NIKA pixels, the 7% average relative frequency shift fixes an upper limit to the OMKID QE. The actual QE of the NIKA pixels, $QE_{\rm NIKA}$, was estimated based on realistic three-dimensional electro-magnetic simulations, room temperature transmission measurements (Roesch et al. 2012), and cold black-body characterisations (Catalano et al. 2020). The measurements indicate that $QE_{\rm NIKA}$ exceeds 80% and that the electromagnetic simulations on LEKID structures are reliable. Considering the 7% average relative frequency shift reported in Fig. 3, and assuming $QE_{\rm NIKA} = 80\%$, the OMKID QE can be estimated in the range 5–6%. An overall QE in the range 5–10% is in line with the performance of existing devices. The optical NEP of the OMKID spectrometer can be estimated from the above figures as follows:

$$\mathrm{NEP}_{\rm OMKID} = \mathrm{NEP}_{\rm NIKA} \times N_{\rm OMKID}/N_{\rm NIKA} \times \delta f_{\rm NIKA}/\delta f_{\rm OMKID},$$

where the correcting factors are the noise ratio and the relative frequency shift. Using this approach, we get $\mathrm{NEP}^{\rm mm} \sim 0.3$ fW Hz$^{-0.5}$ (Fig. 3, panel d).

The two methods give consistent results, confirming also that the sensitivity is currently limited, as is the case for competing devices of this kind, by the relatively poor overall QE.

5. Conclusions

We have developed an on-chip spectrometer based on LEKIDs that is able to cover the astronomically relevant band 85–110 GHz. Our device is characterised by a relatively simple design and fabrication process, compatible with hybridisation on large field-of-view LEKID imaging arrays. The first prototype shows good performance in terms of spectral resolution ($R \approx 300$, as designed) and polarisation selection. The optical sensitivity figures are promising. A significant improvement is possible as the overall efficiency is, according to simulations, limited to 15–45% by the efficiency of the prototype waveguide-microstrip transition.

Acknowledgements. We acknowledge the specific contribution of the engineer G. Garde to the device holder and the overall support of the Cryogenics, Electronics and Nanofab groups at Institut Néel and LPSC. The fabrication of the device described in this paper was conducted at the PTA Grenoble micro-fabrication facility. This work has been partially supported by the French National Research Agency through Grant No. ANR-16-CE30-0019 ELODIS2, the LabEx FOCUS through Grant No. ANR-11-LABX-0013 and the EU's Horizon 2020 research and innovation program under Grant Agreement No. 800923 (SUPERTED).

References

Adam, R., Adane, A., Ade, P. A. R., et al. 2018, A&A, 609, A115
Bourrion, O., Vescovi, C., Catalano, A., et al. 2013, J. Instrum., 8, C12006
Bryan, S., Aguirre, J., Che, G., et al. 2015, J. Low Temp. Phys., 184, 114
Catalano, A., Goupy, J., le Sueur, H., et al. 2015, A&A, 580, A15
Catalano, A., Bideaud, A., Bourrion, O., et al. 2020, A&A, 641, A179
CONCERTO Collaboration (Ade, P., et al.) 2020, A&A, 642, A60
Endo, A., Karatsu, K., Tamura, Y., et al. 2019, Nat. Astron., 3, 989
Faramarzi, F. B., Mauskopf, P., Gordon, S., et al. 2020, J. Low Temp. Phys., 199, 867
Karkare, K. S., Barry, P. S., Bradford, C. M., et al. 2020, J. Low Temp. Phys., 199, 849
Karkare, K. S., Anderson, A. J., Barry, P. S., et al. 2022, J. Low Temp. Phys. 2022, 1
Levy-Bertrand, F., Benoit, A., Bourrion, O., et al. 2021, Phys. Rev. Appl., 15, 044002
Liu, G., Gu, J., Gao, Z., & Xu, M. 2020, Int. J. Radio Freq. Microwave Comput-Aided Eng., 30, e22058
Monfardini, A., & Lagache, G. 2021, Nat. Astron., 5, 970
Monfardini, A., Benoit, A., Bideaud, A., et al. 2011, ApJS, 194, 24
Roesch, M., Benoit, A., Bideaud, A., et al. 2012, ArXiv e-prints [arXiv:1212.4585]
Swenson, L. J., Cruciani, A., Benoit, A., et al. 2010, Appl. Phys. Lett., 96, 263511
Volpert, C. G., Barrentine, E. M., Mirzaei, M., et al. 2022, in Space Telescopes and Instrumentation 2022: Optical, Infrared, and Millimeter Wave, 12180, eds. L. E. Coyle, S. Matsuura, & M. D. Perrin, International Society for Optics and Photonics (SPIE), 121804Z